THE FASEB JOURNAL • RESEARCH • www.fasebj.org

# Ferroportin disease mutations influence manganese accumulation and cytotoxicity

**Eun-Kyung Choi,* Trang-Tiffany Nguyen,* Shigeki Iwase,† and Young Ah Seo*,[1]**

*Department of Nutritional Sciences, University of Michigan School of Public Health, Ann Arbor, Michigan, USA; and †Department of Human Genetics, University of Michigan, Ann Arbor, Michigan, USA

**ABSTRACT: Hemochromatosis is a frequent genetic disorder, characterized by the accumulation of excess iron across tissues. Mutations in the *FPN1* gene, encoding a cell surface iron exporter [ferroportin (Fpn)], are responsible for hemochromatosis type 4, also known as ferroportin disease. Recently, Fpn has been implicated in the regulation of manganese (Mn), another essential nutrient required for numerous cellular enzymes. However, the roles of Fpn in Mn regulation remain ill-defined, and the impact of disease mutations on cellular Mn levels is unknown. Here, we provide evidence that Fpn can export Mn from cells into extracellular space. Fpn seems to play protective roles in Mn-induced cellular toxicity and oxidative stress. Finally, disease mutations interfere with the role of Fpn in controlling Mn levels as well as the stability of Fpn. These results define the function of Fpn as an exporter of both iron and Mn and highlight the potential involvement of Mn dysregulation in ferroportin disease.—Choi, E.-K., Nguyen, T.-T., Iwase, S., Seo, Y. A. Ferroportin disease mutations influence manganese accumulation and cytotoxicity. FASEB J. 33, 2228–2240 (2019). www.fasebj.org**

**KEY WORDS: manganese transport · manganese toxicity · iron metabolism**

Hemochromatosis is a frequent hereditary iron metabolism disorder characterized by the accumulation of excess iron across tissues (1). Untreated hemochromatosis can be fatal due to organ failure. The Online Mendelian Inheritance in Man (OMIM; *https://www.omim.org/*) database classifies 4 types of hemochromatosis (type 1 to type 4) based on inheritance, genetic mutations, and clinical manifestations of the disease. It is well established that hemochromatosis mutations interfere with the function of genes that control cellular iron levels [as reviewed by Powell *et al*. (2)]. Homeostatic iron regulator *HFE* is a cell surface iron sensor, and its mutations account for hemochromatosis type 1. One of the hemochromatosis type 2 genes encodes hepcidin antimicrobial peptide *HAMP*, which regulates the synthesis of a key iron homeostasis factor called hepcidin. Transferrin receptor 2 (*TFR*2) mutations are responsible for hemochromatosis type 3. Transferrin receptor 2, a second receptor for serum transferrin, incorporates transferrin-bound iron from blood into cells (3). Finally, mutations in the *FPN1* gene cause an autosomal dominant form of hemochromatosis type 4 (OMIM 606069), also called ferroportin disease (4).

Ferroportin (Fpn), also known as MTP1, IREG1, or SLC40A1 (UniProt Accession No. Q9NP59; OMIM 604653; *https://www.uniprot.org/*), is a transmembrane protein present in the plasma membrane and is the only known cellular iron exporter that has been identified in mammals (5–7). Fpn is expressed in duodenal enterocytes and absorbs dietary iron, hepatic and splenic iron-recycling macrophages, and hepatocytes, where the transporter can export stored iron when demand is high (6). Fpn is regulated by hepcidin, which internalizes and degrades Fpn, thereby decreasing the iron supply to plasma (8, 9). Similar to other hemochromatosis types, long-term iron overload in ferroportin disease leads to a broad spectrum of pathologic outcomes such as liver damage, including fibrosis and/or cirrhosis, if left untreated.

Currently, >50 heterozygous mutations in the *FPN1* gene have been associated with hemochromatosis type 4 (10). Mutations in the *FPN1* gene can result in 2 subtypes of this condition, type 4A and type 4B, depending on the nature of the mutations. Hemochromatosis type 4A is the classic ferroportin disease characterized by normal-to-low transferrin saturation, which is an indicator of functional blood iron level, and preferential iron retention in macrophages. This classic form of the disease is associated with loss-of-function (LOF) Fpn mutations that interfere with the iron export capability of Fpn. In contrast, hemochromatosis type 4B, also known as nonclassic ferroportin

**ABBREVIATIONS:** apo-Tf, apo-transferrin; DCF, dichlorofluorescein; Fpn, ferroportin; GOF, gain-of-function; $H_2$DCFDA, 2′,7′-dichlorodihydrofluorescein diacetate; HA, hemagglutinin; ICP-MS, inductively coupled plasma mass spectrometry; LOF, loss-of-function; Mn, manganese; MTT, 3-(4,5-dimethylthiazol-2-*yl*)-2,5-diphenyltetrazolium bromide; OMIM, Online Mendelian Inheritance in Man; ROS, reactive oxygen species; siRNA, small interfering RNA; WT, wild type

[1] Correspondence: Department of Nutritional Sciences, University of Michigan School of Public Health, 3850 SPH I, 1415 Washington Heights, Ann Arbor, MI 48109, USA. E-mail: youngseo@umich.edu

doi: 10.1096/fj.201800831R



0892-6638/19/0033-2228 © FASEB

disease, is characterized by high transferrin saturation in the blood along with iron accumulation, preferentially in hepatocytes rather than macrophages. This nonclassic ferroportin disease is associated with the gain-of-function (GOF) mutations that do not impair protein expression at the cell membrane or its iron export activity but rather impair hepcidin-induced Fpn degradation. Consistent with the opposite consequences in blood iron levels, patients with the GOF mutations (type 4B/nonclassic) respond well to the conventional treatment of phlebotomy therapy, whereas patients with the LOF mutations (type 4A/classic) become anemic in response to phlebotomy therapy. No effective treatment is available for hemochromatosis type 4A (4).

Although iron export activity of Fpn has been established in multiple experimental models, including *Xenopus* oocytes and HEK293T cells (5, 7, 11), studies have suggested that Fpn can control cellular manganese (Mn) levels. Using *Xenopus* oocytes, Madejczyk and Ballatori (12) have shown that Fpn-expressing oocytes exported more $^{54}$Mn than control. Meanwhile, another group did not observe detectable Mn export by Fpn in the *Xenopus* oocyte model, possibly due to a low baseline Mn level within the oocytes (13). The roles of Fpn in cellular Mn levels have also been described in mammalian systems. Inducible expression of Fpn in HEK293T cells reduced Mn accumulation and toxicity (14). Fpn expression was elevated when extracellular Mn levels increased in Caco-2 cells, a cell culture model for intestinal absorption (15). However, these studies in mammalian cells did not directly test the efflux of Mn by Fpn. Therefore, the roles of Fpn in Mn regulation remain incompletely understood.

Mn is an essential nutrient that functions as a cofactor for the activity of numerous enzymes in cellular processes (16). However, elevated levels of Mn can be toxic to cells because they increase oxidative stress, impair mitochondrial function, and promote cell death (17, 18). Thus, intracellular Mn levels must be tightly controlled to avoid both excess and insufficiency. Although the role of Fpn in Mn homeostasis is beginning to be appreciated, the impact of ferroportin disease mutations on Mn accumulation and toxicity remains unknown. Thus, the goal of the present study was to define the role of Fpn in Mn regulation and determine the functional consequences of ferroportin disease mutations in cellular Mn levels.

## MATERIALS AND METHODS

### Vector construction and site-directed mutagenesis of Fpn

Human Fpn cDNA was obtained from a cDNA clone (GenBank accession number BC035893; National Center for Biotechnology Information, Bethesda, MD, USA; *https://www.ncbi.nlm.nih.gov/genbank/*). The entire coding region of the wild-type (WT) forms of human Fpn were amplified and tagged at the C terminus with 2 tandem hemagglutinin (HA) epitopes by PCR using primers FWD 5′-CCACCATGACCAGGGCGGGAGATCAC-3′ and Rev 5′-GGCGTAGTCGGGGACGTCGTAGGGGTAGGCGTAGTCGGGGACGTCGTAGGGGTAAACAACAGATGTATTTGCTTG-3′ and inserted into pcDNA3.1/V5-His TOPO vector (Thermo Fisher Scientific, Waltham, MA, USA). Point mutations were introduced into this construct using the QuikChange mutagenesis kit (Agilent Technologies, Santa Clara, CA, USA). The site-directed mutation, orientation, and fidelity of the inserts and incorporation of the epitope tags were confirmed by directed sequencing (University of Michigan DNA Sequencing Core, Ann Arbor, MI, USA).

### Cell culture and the expression of Fpn and its mutants in HEK293T cells

All culture media and supplements were purchased from Thermo Fisher Scientific. Heat-inactivated fetal bovine serum was purchased from MilliporeSigma (Burlington, MA, USA). HEK293T cells and SH-SY5Y cells were grown in DMEM containing 10% fetal bovine serum, penicillin (100 IU/ml), and streptomycin (100 mg/ml) at 37°C in a humidified, 5% $CO_2$ incubator. DNA transfections were performed with Lipofectamine 3000 (Thermo Fisher Scientific) according to the manufacturer's specifications. Cultures were generally transfected 24 h after plating and used 48 h after transfection. For small interfering RNA (siRNA)-mediated gene suppression of Fpn or SLC30A10, SH-SY5Y cells were plated in 6-well plates overnight and then transfected with 50 nM of control siRNA (SIC001-10NMOL; MilliporeSigma), Fpn siRNA (SASI_Hs01_00224698; MilliporeSigma), or SLC30A10 siRNA (SASI_Hs01_00089069; MilliporeSigma) using Lipofectamine 3000 (Thermo Fisher Scientific) as described earlier.

### Immunofluorescence and microscopy

For confocal studies, transfected cells were plated onto glass coverslips and fixed with 4% paraformaldehyde in PBS for 10 min, and immunofluorescence staining was performed as previously described (19–21). To permeabilize the cells, cells were incubated with 0.2% Triton X-100 in PBS for 5 min. Nonspecific binding was blocked with 4% bovine serum albumin in PBS for 30 min, and transfected HA-tagged Fpn-WT or its mutants were detected after incubation with Alexa 488–conjugated anti-mouse HA (90159, 1 μg/ml; BioLegend, San Diego, CA, USA) for 1 h. Rabbit pan-cadherin (1 μg/ml, ab6529; Abcam, Cambridge, United Kingdom) was used as cell surface markers. Detection of pan-cadherin was performed by using an anti-rabbit IgG antibody conjugated to Alexa 568 (1 μg/ml, A11036; Thermo Fisher Scientific) for 20 min. Coverslips were drained, mounted in ProLong Gold (Thermo Fisher Scientific), and sealed with nail polish. Immunofluorescent imaging was performed by using a Nikon Eclipse A-1 confocal microscope (Nikon Instruments, Melville, NY, USA) with a ×60 oil immersion lens. Colocalization analysis was performed after background subtraction through the use of the colocalization function in Fiji by ImageJ (National Institutes of Health, Bethesda, MD, USA), and colocalized pixels were pseudocolored yellow. To quantify the subcellular localization of each mutant with pan-cadherin, statistical analysis of the correlation of the intensity values of green and red pixels in a dual-channel image was performed by using a correlation coefficient (Pearson's coefficient). The value can range from +1 to −1, with +1 indicating a positive correlation, −1 a negative correlation, and 0 indicating no correlation (22).

### Immunoblot analysis

The total lysates were prepared in a hypotonic buffer by using 1% NP-40 plus protease inhibitors (11836153001; Roche, Basel, Switzerland). Protein concentration was determined with the Bradford assay. Samples (30–50 μg) were separated by electrophoresis and transferred to a nitrocellulose membrane (1620115; Bio-Rad, Hercules, CA, USA). The membrane was immunoblotted with

anti-mouse HA antibody (901501; BioLegend), anti-rabbit GPP130 antibody (923801; BioLegend), anti-mouse green fluorescent protein antibody (101536; Santa Cruz Biotechnology, Dallas, TX, USA), and anti-mouse actin (60008-1-Ig; Proteintech, Rosemont, IL, USA). The blots were visualized with infrared anti-mouse or anti-rabbit secondary antibodies, using a Li-Cor Odyssey fluorescent Western blotting system (Li-Cor, Lincoln, NE, USA). Protein expression was quantified by using densitometry (Image Studio Lite; Li-Cor).

### $^{54}$Mn and $^{59}$Fe accumulation and efflux assay

$^{54}$Mn uptake assay was determined as previously described (21, 23, 24). Briefly, HEK293T cells were transfected with empty vector (control), Fpn-WT, or mutants. Two days after transfection, cells were incubated at 37°C for 30 min in serum-free media containing 1 μM $^{54}$Mn. After uptake, cells were washed 3 times with PBS containing 1 mM EDTA to remove any unbound $^{54}$Mn and either directly harvested for intracellular radioactivity or used for the chase part of the experiment. Cells were then transferred to HBSS without $^{54}$Mn and incubated at 37°C for 10 min (chase phase). At the end of the chase, HBSS was collected to assess Mn secreted from cells, and cells were digested to assess intracellular Mn retained. For the $^{59}$Fe uptake assay, HEK293T cells were transfected with empty vector (control) or Fpn-WT. Two days after transfection, cells were incubated at 37°C for 60 min in serum-free medium containing 1 μM $^{59}$Fe and 150 μM L-ascorbic acid. After uptake, cells were washed 3 times with PBS containing iron chelator solution (1 mM bathophenanthroline sulfonate and 1 mM diethylenetriaminepentaacetic acid) to remove any unbound $^{59}$Fe; cells were then either directly harvested for intracellular radioactivity or used for the chase part of the experiment. Cells were then transferred to HBSS containing 10 μM apo-transferrin (apo-Tf) and 6.6 nM soluble human plasma ceruloplasmin without $^{59}$Fe and incubated at 37°C for 120 min (chase phase). Apo-Tf and soluble human plasma ceruloplasmin were added as previously described (25). At the end of the chase phase, HBSS was collected to assess iron secreted from cells, and cells were lysed to assess intracellular iron levels. Radioactivity was determined with a gamma counter and was normalized to the cell protein measured in lysates by using the Bradford assay. The percentage of extracellular metal levels over the total (intracellular + extracellular) metal levels was presented as an indicator for metal export activity.

### Trace element analysis

HEK293T cells transfected with empty vector (control), Fpn-WT, or mutants were analyzed for metals by inductively coupled plasma mass spectrometry (ICP-MS) as previously described (21). Briefly, the cell samples were digested with 2 ml/g total wet weight nitric acid (Aristar Ultra; VWR International, Radnor, PA, USA) for 24 h and then digested with 1 ml/g total wet weight hydrogen peroxide (Aristar Ultra; BDH Chemicals, Poole, United Kingdom) for 24 h at room temperature. The samples were preserved at 4°C until quantification of metals. Ultrapure water was used for final sample dilution.

### Measurement of ferritin

The intracellular ferritin level was measured by using a Human Ferritin ELISA kit (ab108837; Abcam) according to the manufacturer's instructions. Briefly, transfected cells were treated with 20 μM ferric ammonium citrate for 16 h, and cell lysates were then prepared. Samples were incubated with biotinylated ferritin antibody at room temperature, followed by the addition of streptavidin-peroxidase conjugate and chromogen substrate. Samples were read at 450 nm by using a BioTek Synergy HTX Multi-Mode Microplate Reader (BioTek Instruments, Winooski, VT, USA), and values were normalized according to protein concentration.

### Cell viability

Cell viability was measured by the conversion of the dye 3-(4,5-dimethylthiazol-2-*yl*)-2,5-diphenyltetrazolium bromide (MTT; MilliporeSigma) to formazan, as previously described (21, 26). Briefly, the cells were incubated with MTT (0.5 mg/ml) for 3 h, followed by addition of the MTT solvent (isopropyl alcohol containing 0.1 N HCl) to dissolve the formazan. The resulting formazan was assessed spectrophotometrically at 570 nm, and the background was subtracted at 690 nm by using a plate reader (BioTek Instruments).

### Measurement of reactive oxygen species formation

Reactive oxygen species (ROS) levels were measured by using a fluorescent indicator specific for $H_2O_2$ production [2′,7′-dichlorodihydrofluorescein diacetate ($H_2$DCFDA)] as previously described (21). $H_2$DCFDA, a cell-permeant ROS indicator, is nonfluorescent and then converted to highly fluorescent 2′,7′-dichlorofluorescein (DCF) after the removal of the acetate groups by intracellular esterases and ROS-induced oxidation. Cells were incubated with 3 μM DCFH-DA (Thermo Fisher Scientific) for 30 min at 37°C. Fluorescence of DCF (excitation 495 nm, emission 520 nm) was measured at 25°C by using a plate reader.

### Statistical analysis

Results are presented as means ± SD. Statistical comparisons were determined by using Student's *t* test with Prism 7 software (GraphPad Software, La Jolla, CA, USA). Values of $P < 0.05$ were considered statistically significant. Asterisks in graphs, wherever present, denote statistically significant differences.

## RESULTS

### Impact of ferroportin disease mutations on intracellular ferritin levels and localization

Thus far, >50 mutations in Fpn have been identified in hemochromatosis type 4/ferroportin disease (10). To test whether these mutations alter cellular Mn metabolism, we constructed an expression vector encoding human Fpn with a C-terminal HA epitope tag and introduced 9 clinically relevant mutations by site-directed mutagenesis (**Table 1**). Based on previously reported *in vitro* functional results (**Table 2**), we selected 5 ferroportin disease mutations from each of the 2 groups: 5 LOF mutations (G80S, R88G, D157G, D157Y, and V162Δ) and 4 GOF mutations (N144H, N144T, C326S, and S338R). The mutations and their positions in the protein structure are summarized in **Fig. 1*A***. G80S, N144H, and N144T are located in predicted transmembrane domains. R88G, D157G, D157Y, and V162Δ reside in the intracellular domains, whereas C326S and S338R substitutions occur in extracellular domains.

We first sought to confirm the reported roles of Fpn and its LOF and GOF mutants in the regulation of intracellular

TABLE 1. *Summary of clinically known ferroportin disease mutations considered in the current study*

| Mutation | Serum ferritin (μg/L) | Transferrin saturation (%) | Clinical phenotype | Reference |
|---|---|---|---|---|
| WT | 15–200 F; 40–300 M | 15–45 both | | 56 |
| G80S | 519–702 F; 1200–3109 M | 24–47 F; 35 M | Loss of function | 29 |
| | 1540–4420 M | 42–60 M | | 57 |
| | 649–2434 M | 25–28 F; 28–32 M | | 58 |
| | 1233–2690 F; 966–1530 M | | | 43 |
| R88G | 4129–4910 F; 2840 M | 39–54 F | Loss of function | 29 |
| | 8.2–44.5[a] | 11–79[a] | | 30 |
| | 2200 M | | | 59 |
| D157G | 1590–6000 F; 4459 M | 20–53 F; 35 M | Loss of function | 29 |
| | 4069 M | 44 M | | 60 |
| D157Y | 2213 M | 35 M | Loss of function | 29 |
| V162Δ | 977–2578 F; 71.2–2268 M | 14–35 F; 25–32 M | Loss of function | 29 |
| | 4886 F; 2558 M | | | 58 |
| N144H | 31–2179[a] | 16–88.6[a] | Gain of function | 61 |
| | 141.8–3108 M | 50.4–100 M | | 62 |
| N144T | 2937 M | 80 M | Gain of function | 63 |
| C326S | 151–299 F | | Gain of function | 64 |
| | 69–394 M | 84–97 F; 86–94 M | | 65 |
| S338R | 1990 M | 90 M | Gain of function | 33 |

F, female; M, male. [a]Did not specify sex.

iron levels by measuring cytosolic iron storage protein ferritin (Fig. 1*B*). Following the export of intracellular iron by Fpn, intracellular iron should be depleted, thereby leading to a reduction in intracellular ferritin concentrations (27–29). Due to a low Fpn mRNA expression level, HEK293T cells were ideal for detecting the impact of Fpn cDNA overexpression. HEK293T cells were transiently transfected with expression plasmids for control, Fpn-WT, or mutants and then incubated with 20 μM ferric ammonium citrate. Subsequently, the intracellular ferritin levels were determined by using ELISA. The expression of Fpn-WT resulted in a reduction of ~67% in intracellular ferritin concentrations compared with the control cells. As expected from previous reports (27–30), cells expressing LOF mutants, G80S, R88G, D157G, D157Y, or V162Δ were iron loaded, whereas the cells expressing GOF mutants N144H, N144T, C326S, or S338R were iron depleted, similar to those expressing Fpn-WT.

Previous research has shown that LOF Fpn mutants failed to localize at the plasma membrane (29–31). Thus, we next validated the reported mislocalization of Fpn mutants. HEK293T cells expressing HA-tagged Fpn-WT and mutants were costained with HA and the cell surface marker pan-cadherin, and they were then analyzed by using confocal microscopy (Fig. 1*C*). As expected, Fpn-WT exhibited significant overlap with the cell surface marker pan-cadherin in addition to some intracellular staining. The LOF mutants G80S, R88G, D157G, D157Y, and V162Δ showed substantially weaker or undetectable costaining with pan-cadherin at the cell surface. In contrast, the GOF mutants N144H, N144T, C326S, and S338R displayed a similar staining pattern as the Fpn-WT. Our measurement of Pearson's correlation coefficient (19, 22) revealed statistically significant decreases in HA−cadherin colocalization within the LOF mutant-expressing cells compared with WT-expressing cells ($P < 0.01$, Fig. 1*D*). No significant differences were found between the GOF mutant-expressing cells, except C326S ($P < 0.05$). Taken together, these data indicate that the behavior of LOF and GOF mutants in our experimental systems is similar to that of previous reports (28, 29, 31–33).

TABLE 2. *Summary of* in vitro *functional results of ferroportin disease mutations considered in the current study*

| Mutation | Cellular localization | Iron transport | Functional results | Reference |
|---|---|---|---|---|
| WT | Plasma membrane | Normal | | 28 |
| G80S | Plasma membrane | Impaired | Loss of function | 43 |
| | Intracellular | | | 29 |
| R88G | Intracellular | Impaired | Loss of function | 30 |
| | Plasma membrane | | | 29 |
| D157G | Intracellular | Impaired | Loss of function | 42, 29, 31 |
| D157Y | Intracellular | Impaired | Loss of function | 29 |
| V162Δ | Intracellular | Impaired | Loss of function | 28, 31 |
| N144H | Plasma membrane | Normal | Gain of function | 28, 42 |
| N144T | Plasma membrane | Normal | Gain of function | 32 |
| C326S | Plasma membrane | Normal | Gain of function | 32 |
| S338R | Plasma membrane | Normal | Gain of function | 33 |

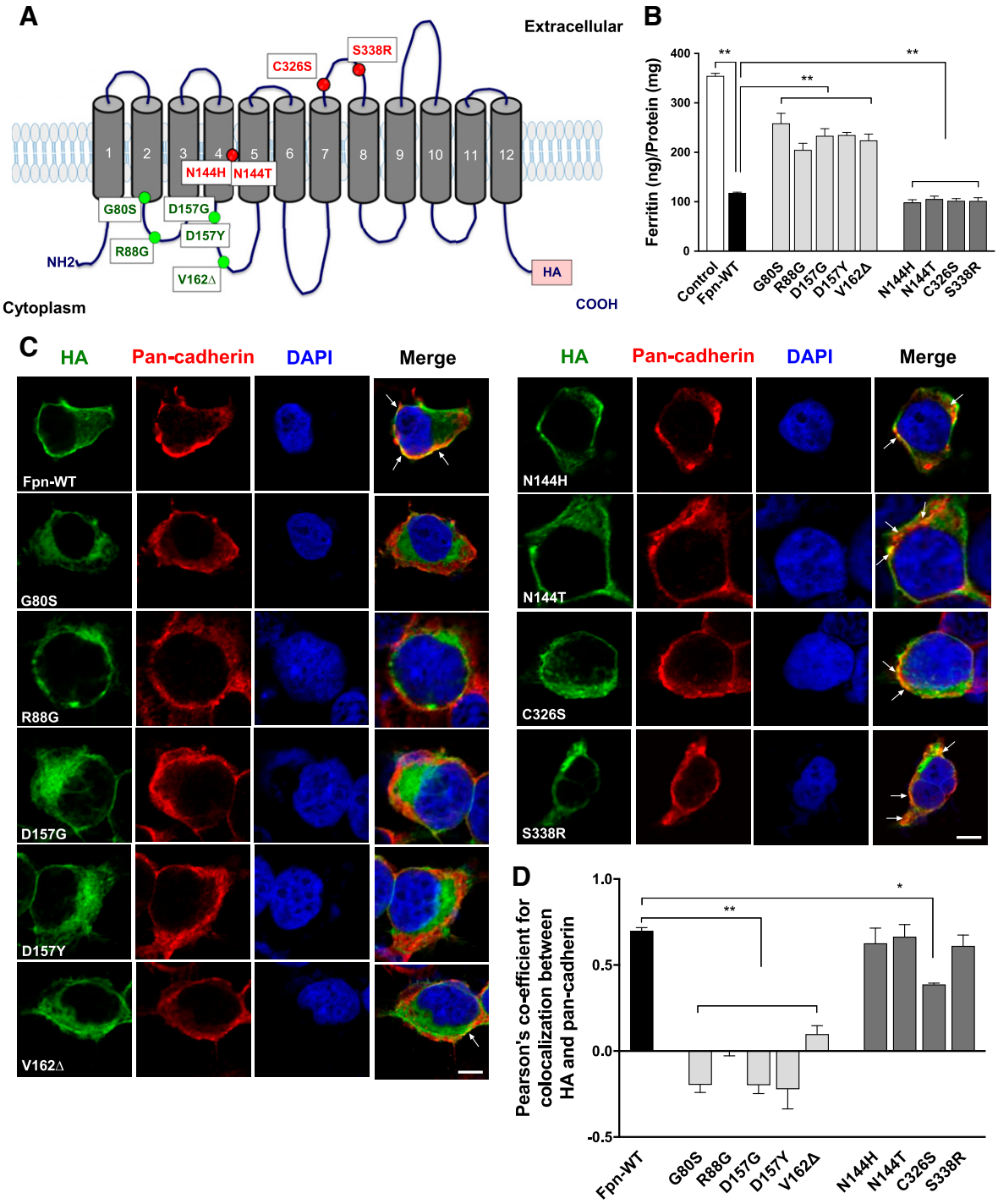


**Figure 1.** Effect of ferroportin disease mutations on intracellular ferritin levels and localization. *A*) A model of predicted topology of Fpn based on previous studies (33, 55). Twelve transmembrane domains, intracellular $NH_2$ and COOH terminus, and the COOH terminal HA tag used in these experiments are described. Ten mutations identified in patients with ferroportin disease examined in this study and the corresponding locations of these mutations are indicated as green text for LOF mutations and red text for GOF mutations. *B*) HEK293T cells were transfected with empty vector (control), Fpn-WT, or Fpn mutants. After 48 h of transfection, the cells were treated with ferric ammonium citrate (20 μM) for 16 h, and intracellular ferritin levels were measured by using ELISA. The values were normalized according to protein concentration. *C*) Representative confocal images of HEK293T cells expressing the HA-tagged Fpn-WT and its mutants are shown. To detect Fpn-WT and its mutants, the cells were incubated with Alexa 488–conjugated anti-mouse HA antibody (green). To detect the cell surface, the cells were coincubated with anti–pan-cadherin antibody followed by Alexa Fluor 568–conjugated secondary antibody (red). Merged images of HA and pan-cadherin reveal areas of colocalization (yellow), indicated by arrows. Blue color indicates nuclei counterstained with DAPI. Scale bar, 10 μm. *D*) Quantification of Pearson's coefficient for colocalization between HA and calnexin from *C*. Results are means ± SD of 3 independent experiments. The value of Pearson's coefficient can range from 1 to −1, with 1 indicating complete positive correlation and −1 a negative correlation, with zero indicating no correlation. $*P < 0.05$, $**P < 0.01$ between control vector *vs.* Fpn-WT or between Fpn-WT *vs.* its mutants (Student's *t* test).

## LOF mutations reduce Fpn stability

Although a previous study reported mislocalization of Fpn by the LOF mutations found in ferroportin disease, the stability of mutant proteins remains unknown. To address this issue, we performed immunoblot analysis of Fpn recombinant proteins expressed in HEK293T cells. As shown in **Fig. 2**, cells expressing Fpn-WT had a prominent band at ~70 kDa and a less intense band at ~60 kDa. Slower migration of the 70 kDa form in the gel has been explained by *N*-linked glycosylation of the protein (34). The LOF mutations G80S, R88G, D157G, D157Y, and V162Δ resulted in substantially reduced protein levels (Fig. 2*A*). In particular, V162Δ showed increased accumulation of a smaller molecular mass form. The GOF mutations did not tend to alter protein levels, with one exception: S338R exhibited reduced protein levels compared with WT. Green fluorescent protein was included as a control of transfection efficiency, indicating equal transfection efficiencies of WT and Fpn mutants. These data indicate that failure of localization at the plasma membrane (Fig. 1*C, D*), as well as the reduced overall protein level (Fig. 2*B*), collectively lead to the inability of the LOF mutants to reduce the intracellular iron levels seen in Fig. 1*B*.

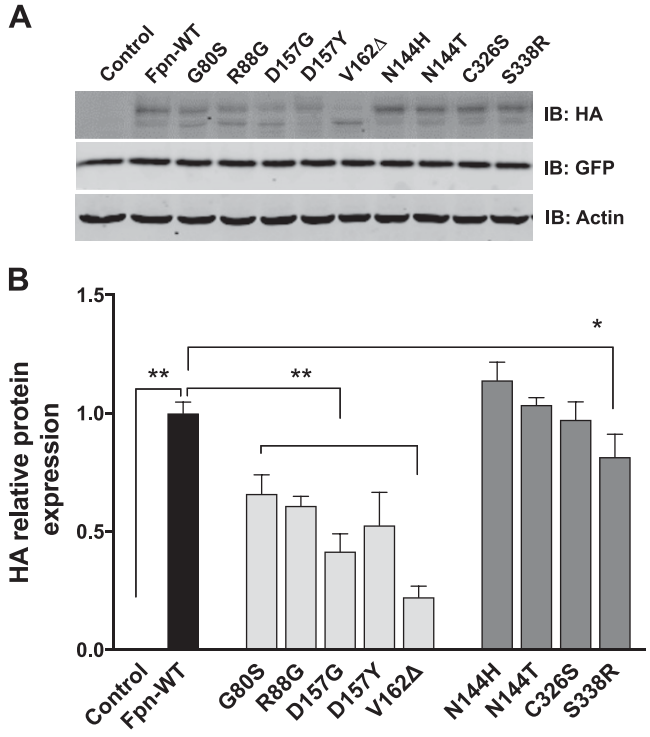


**Figure 2.** Expression of Fpn-WT and mutations associated with ferroportin disease. *A*) Representative immunoblot of HA-tagged Fpn-WT and other mutants in total cell lysates isolated from cells expressing empty vector (control), Fpn-WT, or Fpn mutants. Green fluorescent protein (GFP) is included as a control for transfection efficiency. Immunoblot of actin was used as a loading control. *B*) Quantification of HA relative protein after normalization with actin. Results are means ± SD ($n$ = 3 samples/group) of 3 independent experiments. $*P < 0.05$, $**P < 0.01$ between control vector *vs.* Fpn-WT or between Fpn-WT *vs.* its mutants (Student's $t$ test).

## Impact of ferroportin disease mutations on intracellular Mn levels

Having established the correct behavior of LOF and GOF mutants in iron export, we proceeded to probe the impact of these mutations on cellular Mn levels. We first measured Mn levels in cells expressing a control construct or Fpn-WT. Mn measurements were performed by using ICP-MS and after exposure of cells to 0–500 μM Mn for 16 h. Such levels of Mn are not toxic to cells (26). Intracellular Mn levels in cells expressing Fpn-WT were lower than those in control cells (**Fig. 3*A***), indicating that the expression of Fpn-WT reduces cellular Mn levels. We also noted that intracellular iron levels in cells expressing Fpn-WT tended to be lower than those in control cells after exposure to 125 or 250 μM Mn, although this reduction did not reach statistical significance (Fig. 3*B*). The trend of reduced intracellular iron levels may reflect the iron-exporting activity of Fpn in the absence of higher iron exposure. We further tested whether the Fpn mutant expression alters intracellular Mn levels. As shown in Fig. 3*C*, the expression of the LOF mutants G80S, R88G, D157G, D157Y, and V162Δ failed to reduce Mn levels compared with Fpn-WT expression ($P < 0.01$). In contrast, the expression of the GOF mutants N144H, N144T, C326S, and S338R showed similar levels of cellular Mn compared with cells expressing Fpn-WT, indicating no significant accumulation of Mn in the cells. No differences were observed in cellular iron levels in cells expressing Fpn-WT or its mutants under these conditions (Fig. 3*D*).

We next measured levels of the Mn sensor Golgi protein GPP130 (35). An increase in intra-Golgi Mn is known to induce GPP130 trafficking from the Golgi to late endosomes and lysosomes, leading to GPP130 degradation. Thus, we hypothesized that if Fpn-WT reduces intracellular Mn levels, it would reduce the transport of Mn into the Golgi, in turn inhibiting GPP130 degradation. The stability of GPP130 was assessed with and without $MnCl_2$ treatment by immunoblot. As expected, the level of GPP130 was significantly reduced in control cells treated with Mn (Fig. 3*E*). Furthermore, this Mn-induced degradation was blocked in cells expressing Fpn-WT. Quantification indicated that ~57% of GPP130 was lost after Mn treatment in control cells, whereas no significant decrease was seen in Fpn-WT–expressing cells (Fig. 3*F*). Importantly, expression of the LOF mutants G80S, R88G, D157G, D157Y, and V162Δ did not prevent the Mn-induced loss of GPP130, whereas expression of the GOF mutants N144H, N144T, C326S, and S338R blocked GPP130 degradation. These results indicate that the overexpression of Fpn-WT and the GOF mutants resulted in Mn depletion in the cells, whereas the LOF mutations abrogated such an effect of Fpn.

## Fpn is a Mn exporter, and disease mutations interfere with its activity

To further define the roles of Fpn in Mn regulation and the impact of disease mutations, we administered radioactively labeled $^{54}Mn$ in cell culture media and then measured the accumulation of Mn within cells overexpressing Fpn-WT or mutants. The overexpression of Fpn-WT resulted in a decrease of ~45% ($P < 0.01$) in intracellular

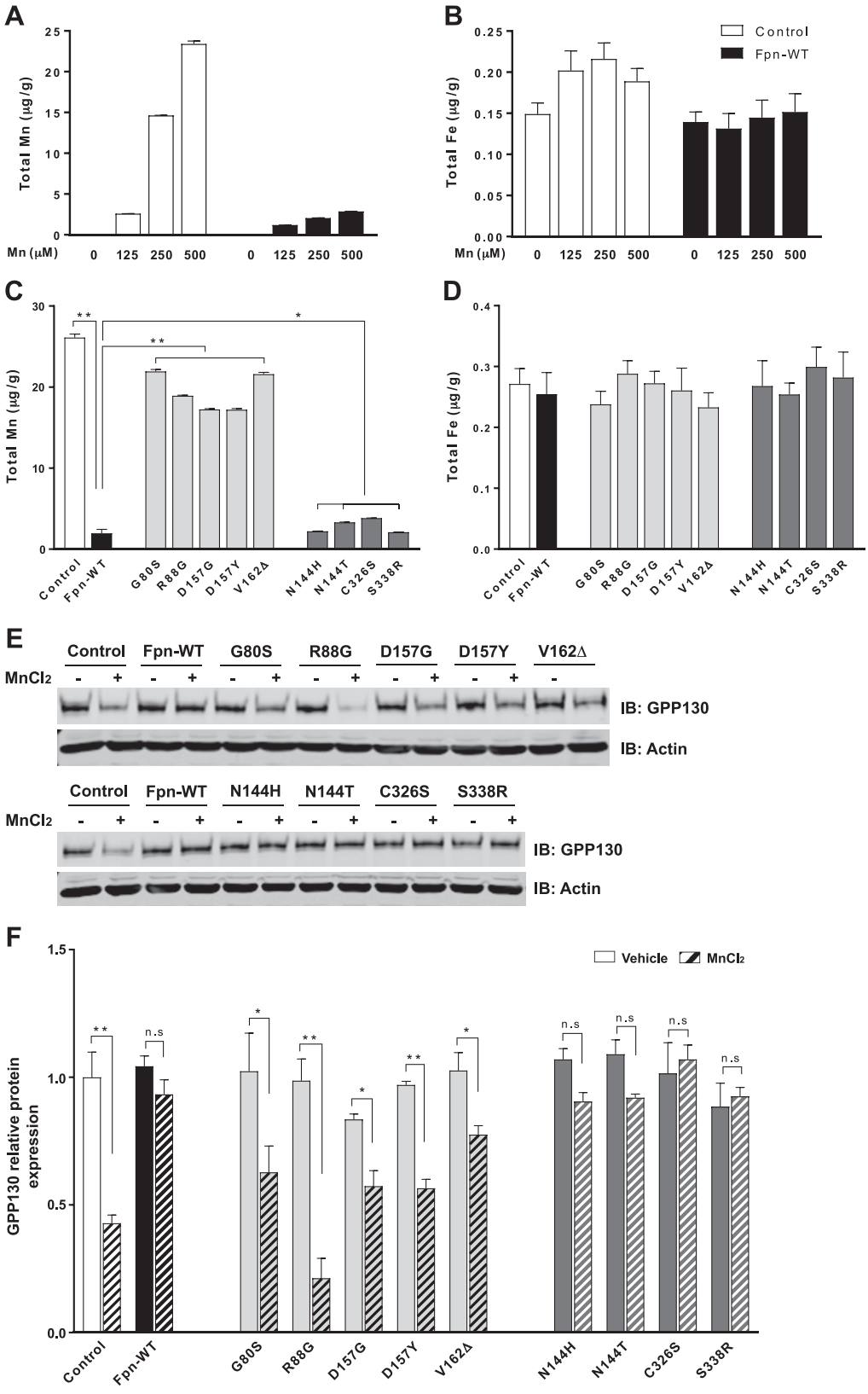


**Figure 3.** Effect of ferroportin disease mutations on intracellular Mn levels. *A*, *B*) HEK293T cells were transfected with empty vector (control) or Fpn-WT for 48 h. After treatment with the indicated amounts of Mn for 16 h, intracellular metal levels, including Mn (*A*) and iron (*B*), were measured by using ICP-MS. *C*, *D*) HEK293T cells were transfected with Fpn-WT or other mutants for 48 h. After treatment with 500 μM Mn for 16 h, intracellular metal levels, including Mn (*C*) and iron (*D*), were measured by using ICP-MS. *E*) Representative immunoblot of GPP130 in total cell lysates isolated empty vector (control), Fpn-WT–, or its mutant-expressing cells incubated with 200 μM $MnCl_2$ for 24 h. Equal loading was verified by immunoblotting with actin antibody. *F*) Quantification of GPP130 relative protein after normalization with actin. Results are means ± SD ($n = 3$ samples/group) of 3 independent experiments. $^*P < 0.05$, $^{**}P < 0.01$ *vs.* vehicle (Student's *t* test). N.s., not significant.

$^{54}$Mn levels in the cells compared with control cells (**Fig. 4*A***). The LOF mutants displayed significantly higher $^{54}$Mn levels compared with Fpn-WT ($P < 0.01$), indicating no effect in reducing Mn levels in those cells. In contrast, the overexpression of GOF mutants led to reduced $^{54}$Mn accumulation, similar to Fpn-WT.

The decrease in intracellular Mn levels and $^{54}$Mn accumulation in Fpn-WT–expressing cells can be caused by either an increased Mn efflux or an impaired Mn uptake. To segregate between these possibilities, pulse-chase assays were performed. Cells expressing control or Fpn-WT constructs were transiently treated with $^{54}$Mn for 30 min

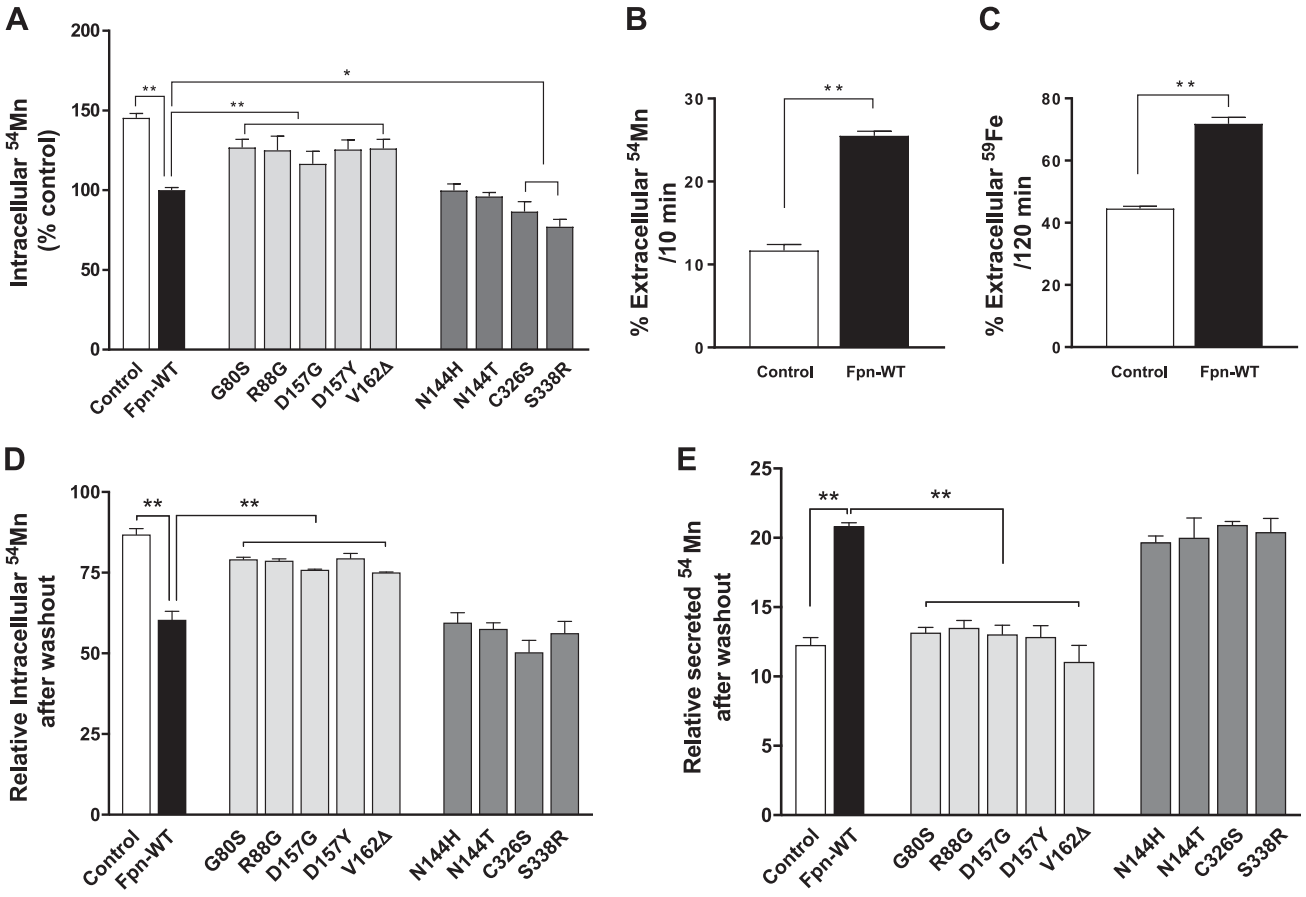


**Figure 4.** Effect of ferroportin disease mutations on accumulation and efflux of $^{54}$Mn. *A*) HEK293T cells were transfected with control, Fpn-WT, or mutants for 48 h and then incubated at 37°C for 30 min in the presence of 1 μM of $^{54}$Mn. Cells were chilled on ice and washed with ice-cold PBS containing 1 mM EDTA; cell-associated radioactivity was determined by using a gamma counter and was normalized to control vector–expressing cells. Data represent means ± SD ($n$ = 3 samples/group). *B, C*) HEK293T cells were transfected with either control or Fpn-WT for 48 h, and the pulse-chase assay for Mn (*B*) and iron (*C*) was performed as described in Materials and Methods. Percentage of extracellular metal levels over the total (intracellular + extracellular) metal levels after the indicated duration of chase period is plotted. Data represent means ± SD ($n$ = 3 samples/group). *D, E*) HEK293T cells were transfected with control, Fpn-WT, or mutants for 48 h, and the Mn pulse-chase assay was performed as described earlier. Intracellular radioactivity retained and secreted after chase was normalized to 100 for control cells. Results are means ± SD ($n$ = 3 samples/group) of 3 independent experiments. *$P < 0.05$, **$P < 0.01$ between control vector *vs.* Fpn-WT or between Fpn-WT *vs.* its mutants (Student's $t$ test).

and then incubated with metal-free media for an additional 10 min. At the end of the metal-free incubation, the amount of Mn retained in the cells and released into the medium was measured by using a gamma counter. Compared with control cells, Fpn-WT–expressing cells retained less intracellular Mn and secreted more Mn into the media (Fig. 4*B*), indicating the increase of Mn efflux by Fpn-WT overexpression. Similarly, in the pulse-chase assays using $^{59}$Fe (see the Materials and Methods section for details), Fpn-WT–expressing cells secreted more iron into the media than control cells (Fig. 4C). Taken together, these data indicate that Fpn exports both Mn and iron with comparable efficiency.

We then examined the efflux activity of cells expressing Fpn mutants. Importantly, there was no difference in the amount of Mn retained within the intracellular compartment or released into the medium between control cells and cells expressing the LOF mutants (Fig. 4*D, E*). The GOF mutants displayed WT-equivalent Mn efflux activity. Taken together, these data show that Fpn can export Mn from cells into extracellular space. In addition, the LOF mutants, which are incapable of down-regulating intracellular iron levels, were also defective in Mn efflux. In contrast, the GOF mutations do not influence exports of either iron or Mn.

## Ferroportin disease mutations influence Mn cytotoxicity

Elevated cellular levels of Mn can result in cytotoxicity and increased oxidative stress (17, 18). The accumulation of Mn by Fpn overexpression prompted us to test whether the expression of ferroportin disease mutants would affect Mn-induced cytotoxicity. We first treated HEK293T cells expressing Fpn-WT or control cells with Mn 0, 0.5, and 1 mM for 16 h and then measured their viability by using the MTT assay. In control cultures, the viability of cells treated with 0.5 or 1 mM was ~79% and ~41%, respectively (**Fig. 5*A***). Importantly, expression

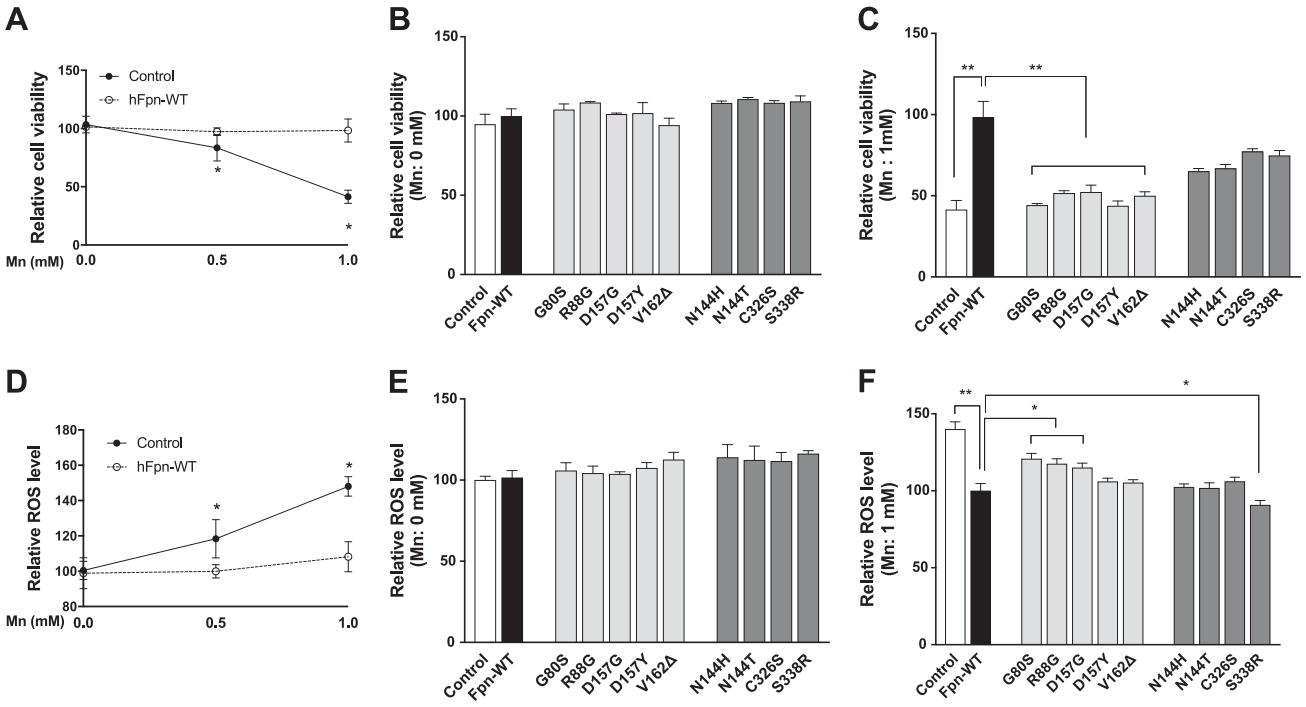


**Figure 5.** Effect of ferroportin disease mutations on Mn cytotoxicity. *A*) HEK293T cells were transfected with control or Fpn-WT. Two days after transfection, cells were exposed to 0.5 and 1 mM of $Mn^{2+}$ for 16 h. Cell viability was determined by using the MTT assay. *B*, *C*) HEK293T cells expressing control, Fpn-WT, or its mutants were left untreated (*B*) or exposed (*C*) to 1 mM of $Mn^{2+}$ for 16 h. Cell viability was determined by using the MTT assay. *D*) HEK293T cells were transfected with control or Fpn-WT. Two days after transfection, cells were exposed to 0.5 and 1 mM of $Mn^{2+}$ for 16 h. Intracellular ROS formation was measured by using DCF fluorescence. *E*, *F*) HEK293T cells expressing control, Fpn-WT, or its mutants were left untreated (*E*) or exposed (*F*) to 1 mM of $Mn^{2+}$ for 16 h. Intracellular ROS formation was measured by using DCF fluorescence. Data represent means ± SD as a percentage of Fpn-WT ($n = 5$ samples/group). $^*P < 0.05$, $^{**}P < 0.01$ between control vector *vs.* Fpn-WT or between Fpn-WT *vs.* its mutants (Student's *t* test). Similar results were obtained in at least 3 independent experiments.

of Fpn-WT did not have any effect on cell viability without Mn treatment, although it protected against the Mn-induced reduction of cell viability. In the absence of Mn treatment, disease mutant expression also did not influence the MTT assay values (Fig. 5*B*). However, after Mn treatment, the viability of cells expressing the LOF mutants was significantly reduced by 46–63% compared with Fpn-WT, whereas the GOF mutants exhibited a protective effect against Mn-induced cytotoxicity, similar to Fpn-WT (Fig. 5C).

To test whether the observed Mn cytotoxicity by ferroportin disease mutations involves ROS production, ROS levels were measured by using fluorescent indicators specifically for $H_2O_2$ production ($H_2$DCFDA). $H_2$DCFDA is converted to highly fluorescent 2′,7′-dichlorofluorescein (DCF) following the removal of the acetate groups by intracellular esterases and ROS-induced oxidation. In control cultures, Mn treatment in increasing concentrations led to significantly higher DCF fluorescence (~18–48%) (Fig. 5*D*). Expression of Fpn-WT protected against ROS production that is induced by Mn but not under the absence of Mn. This Mn-dependent protective effect was weaker in the 3 LOF mutants G80S, R88G, and D157G and not observed in the 2 LOF mutants D147Y and V162Δ (Fig. 5*E, F*). In contrast, all the GOF mutants exhibited a protective effect against Mn-induced oxidative stress (Fig. 5*F*). Taken together, these data indicate that expression of Fpn-WT and the GOF mutants protect cells from Mn cytotoxicity and Mn-induced oxidative stress, whereas the LOF mutants fail to exert such a protective function.

## Knockdown of Fpn increases intracellular Mn levels and exacerbates Mn cytotoxicity

In addition to the effects of Fpn-WT overexpression in HEK293T cells, we sought to test whether endogenous Fpn is necessary for maintaining lower Mn levels in the cells. We took advantage of the endogenous expression of Fpn in SH-SY5Y human neuroblastoma cells. SH-SY5Y cells are a third-generation subclone of the SK-SN-SH dopaminergic neuroblastoma cell line derived from the brain (36) and have been extensively used for studies on Mn toxicity, mitochondrial dysfunction, and neuronal cell death induced by oxidative stress (26, 37, 38). To test the effect of Fpn depletion on the cell viability, we used siRNA to knock down Fpn in SH-SY5Y cells. RT-PCR analysis showed that Fpn is effectively reduced by ~76% ($P < 0.01$) compared with cells transfected with a control siRNA, which should not target any human gene (**Fig. 6*A***). Knockdown of Fpn did not affect cell viability in the absence of Mn (Fig. 6*B*). However, after a 16 h exposure to 0.25 and 0.5 mM Mn, the viability of Fpn-depleted cells was significantly less than that of cells transfected with the control siRNA.

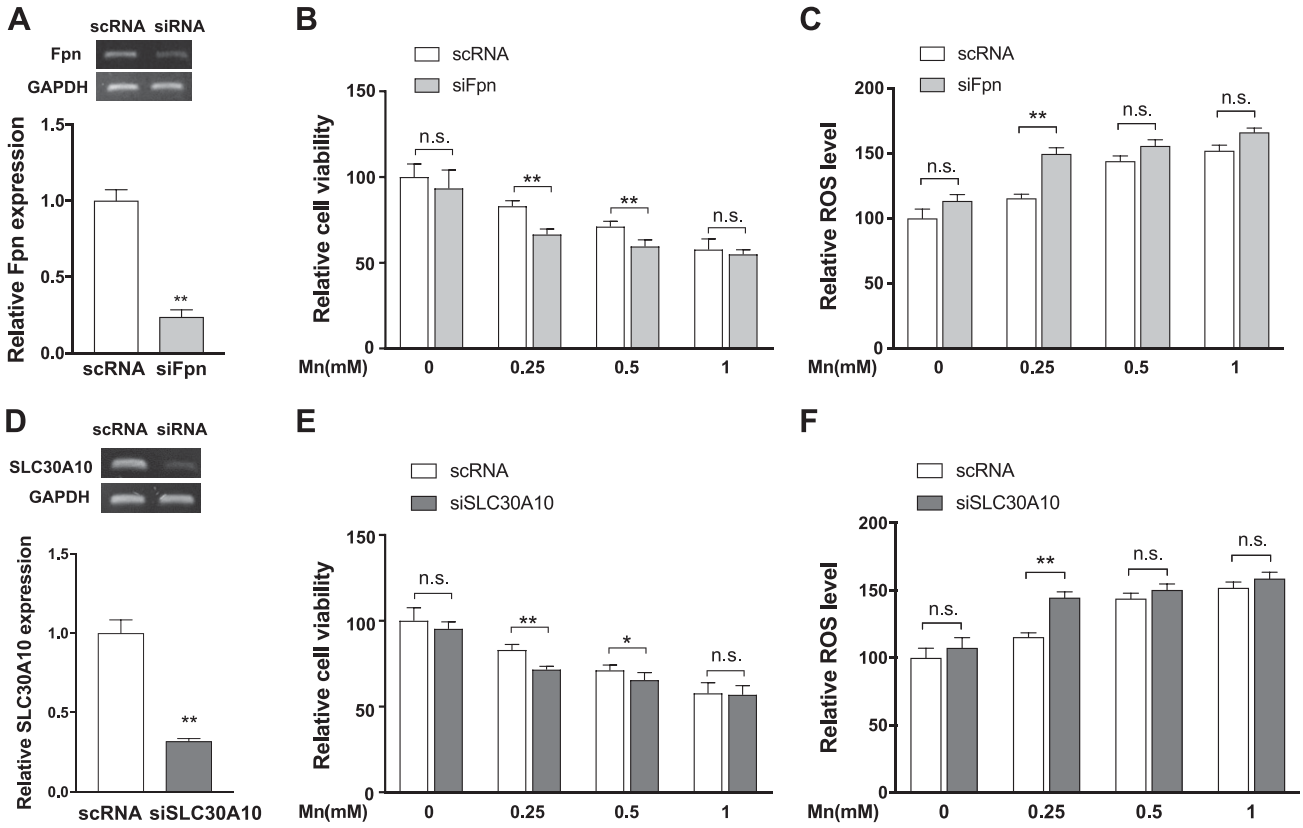


**Figure 6.** Fpn protects against Mn-induced toxicity in dopaminergic SH-SY5Y cells. *A*, *D*) SH-SY5Y cells were transfected with control (scRNA) or anti-Fpn siRNAs (siFpn) or anti-SLC30A10 siRNAs (siSLC30A10). Down-regulation of siFpn (*A*) or siSLC30A10 (*D*) was confirmed by semi-quantitative RT-PCR 48 h after the transfection of each siRNA. *B*, *E*) Twenty-four hours after knockdown, cells were left untreated or exposed to $Mn^{2+}$ for an additional 16 h. Cell viability was assessed by using the MTT assay. *C*, *F*) Twenty-four hours after knockdown, cells were left untreated or exposed to $Mn^{2+}$ for an additional 16 h. Intracellular ROS formation was measured by using DCF fluorescence. Data represent means ± SD ($n$ = 6–8 samples/group). $^{*}P < 0.05$, $^{**}P < 0.01$ *vs.* scRNA-transfected cells (Student's $t$ test). Similar results were obtained in at least 3 independent experiments. N.s., not significant.

Furthermore, the knockdown of Fpn significantly increased $H_2O_2$ production after a 16 h exposure to 0.25 mM Mn (Fig. 6*C*). The knockdown results complement our overexpression studies and indicate that Fpn mediates Mn detoxification.

Studies have shown that SLC30A10 is a cell surface–localized, Mn-efflux transporter (39, 40). To evaluate the contribution of endogenous SLC30A10 in SH-SY5Y cells, we compared the mRNA levels of endogenous Fpn and SLC30A10 in SH-SY5Y cells. The reported RNA-seq data of SH-SY5Y cells indicated that Fpn expression was ~12-fold higher than SLC30A10 (1.85 *vs.* 0.15 fragments/kb of exon model per million mapped reads) (41). To test the effect of SLC30A10 depletion on cell viability, we used siRNA to knock down SLC30A10 in SH-SY5Y cells. RT-PCR analysis revealed that SLC30A10 is effectively reduced by ~70% ($P < 0.01$) (Fig. 6*D*). Knockdown of SLC30A10 did not affect cell viability in the absence of Mn (Fig. 6*E*). However, the knockdown of SLC30A10 significantly decreased cell viability after a 16 h exposure to 0.25 and 0.5 mM Mn. Furthermore, the knockdown of SLC30A10 significantly increased $H_2O_2$ production after a 16 h exposure to 0.25 mM Mn (Fig. 6*F*). These results indicate that similar to Fpn, SLC30A10, despite its low-level expression, can mediate Mn detoxification in SH-SY5Y cells.

## DISCUSSION

The present report describes the first *in vitro* functional analysis of human Fpn mutations in Mn accumulation and cytotoxicity Results are summarized in **Table 3**. We initially found differential consequences of these mutations on the cellular localization and stability of Fpn by examining the behavior of 5 LOF mutants and 4 GOF mutants of Fpn in HEK293T cells. Studies have shown that the LOF mutations, which lead patients to exhibit the classic phenotype of Kupffer cell iron accumulation, affect the localization of Fpn on the cell surface. Consistently, several studies reported intracellular localization of the G80S, R88G, D157G, D157Y, and V162Δ Fpn mutants (28–31, 42). However, other studies found localization of G80S (43), R88G (29), D157G, and V162Δ (44), primarily at the cell surface. Our cellular localization studies supported the notion that the LOF mutants are localized intracellularly, although some cell surface staining was detected. These somewhat inconsistent observations may be partially explained by the

TABLE 3. *Summary of in vitro functional studies of ferroportin disease mutations*

| Mutation | Cellular localization | Intracellular Mn | GPP130 degradation | $^{54}$Mn accumulation | $^{54}$Mn efflux | Mn-induced cell toxicity | Mn-induced ROS |
|---|---|---|---|---|---|---|---|
| WT | Plasma membrane | Normal | Blocked | Decreased | Increased | Protective | Reduced |
| G80S | Intracellular | Increased | Not blocked | Increased | Decreased | Not protective | Increased |
| R88G | Intracellular | Increased | Not blocked | Increased | Decreased | Not protective | Increased |
| D157G | Intracellular | Increased | Not blocked | Increased | Decreased | Not protective | Increased |
| D157Y | Intracellular | Increased | Not blocked | Increased | Decreased | Not protective | Reduced |
| V162del | Intracellular | Increased | Not blocked | Increased | Decreased | Not protective | Reduced |
| N144H | Plasma membrane | Normal | Blocked | Decreased | Increased | Protective | Reduced |
| N144T | Plasma membrane | Normal | Blocked | Decreased | Increased | Protective | Reduced |
| C326S | Plasma membrane/ intracellular | Normal | Blocked | Decreased | Increased | Protective | Reduced |
| S338R | Plasma membrane | Normal | Blocked | Decreased | Increased | Protective | Reduced |

use of different cell lines and the presence or absence of cycloheximide, an inhibitor of protein synthesis, in the assay system (33). In contrast, with regard to the GOF mutations that lead to the nonclassic phenotype of hepatocyte iron accumulation, most studies have shown consistent results of cell surface staining, similar to our observation. In addition to the mislocalization, we found that LOF mutants but not GOF mutants were unstable (Fig. 2). Thus, overall reduction of Fpn protein levels by the mutations might be another contributing factor to classic ferroportin disease.

In this study, we provided several lines of evidence for Fpn's roles in Mn export and the deleterious consequences of disease mutations. First, we described the decreased intracellular Mn levels upon Fpn-WT overexpression by ICP-MS (Fig. 3*A–D*). Second, we validated the intracellular Mn levels by performing the GPP130 degradation assay (Fig. 3*E, F*). Third, we showed that the decrease in intracellular Mn levels in Fpn-WT and the GOF mutants was due to an increase in Mn efflux (Fig. 4). Fourth, Fpn-WT overexpression was protective to Mn-induced cell toxicity and ROS production, whereas Fpn depletion sensitized cells to Mn-dependent oxidative stress (Figs. 5 and 6). Direct measurement of iron efflux has been difficult in mammalian cells. In this study, we were able to detect Fpn-mediated iron efflux using the modified efflux assay (Fig. 4*C*). Based on our pilot experiments, we found that iron requires longer durations of both pulse and chase phases than Mn (data not shown). The differences can be explained by the distinct cellular trafficking mechanisms of the 2 metals. Once inside cells, iron is either deposited in ferritin or incorporated into the mitochondria for heme metabolism and synthesis of iron-sulfur clusters. Thus, iron is not readily available for export, and the export activity of Fpn is dependent on the iron's metabolic response. In contrast, Mn exists in a more labile pool that is readily available for export and is independent of the iron's metabolic response. Because of these differences, we cannot formally compare efflux rate of the 2 metals by Fpn in any cell-based assays. As such, it remains unclear whether Fpn prefers one metal over the other in general or in certain contexts. Nonetheless, our data show that Fpn can export both Mn and iron, and the disease mutations influence export activities of both metals. Further studies will be required to test whether there are key functional amino acids of Fpn that specifically contribute to iron and Mn export activity.

With regard to disease mechanisms, it is important to note that our overexpression experiment and knockdown study do not accurately generalize to the status in patient cells, as disease mutations are heterozygous. It has been proposed that the mutant Fpn protein can act as a dominant negative form over the WT-Fpn (10). Although the present study does not rule out the dominant negative mechanisms, it provides evidence that patient mutations negatively affect the intrinsic activity of Fpn as an exporter of iron and Mn. In a recent study, we characterized flatiron mice, in which Fpn carries the heterozygous H32R mutation and fails to localize at the plasma membrane (26). Flatiron mice display lower Mn levels in the blood and liver and Mn accumulation in the brain (26, 45). Collectively, these observations led us to predict that the classic ferroportin disease/hemochromatosis type 4A, which has been deemed to be solely an iron-overload condition, involves Mn dysregulation.

It is noteworthy that Mn overload preferentially affects the brain (46). Exposure to elevated levels of Mn results in metal accumulation in specific brain regions associated with parkinsonian motor dysfunction (47, 48). In addition to macrophages of the reticuloendothelial system, intestinal duodenum, and hepatocytes (6), Fpn is ubiquitously expressed in the brain, including neurons, astrocytes, the endothelial cells of the blood–brain barrier, oligodendrocytes, the choroid plexus, and ependymal cells (49, 50). Genetic mutations in *S\LC30A10*, a cell-surface Mn exporter gene, were reported in a new form of Mn-induced parkinsonism (51, 52). SLC30A10 is highly expressed in the liver and brain tissues (53) and protects cells against Mn toxicity (39, 54) (Fig. 6). It remains unknown where and how Fpn and SLC30A10 interplay in response to the brain's demands for metal. To date, no neurologic symptoms have been reported in patients with ferroportin disease. Our study raises the possibility that patients with ferroportin disease mutations may be more susceptible to Mn neurotoxicity. Further studies are warranted to evaluate the relevance of ferroportin disease mutations to Mn metabolism and neurotoxicity associated with metal exposure in the human population. FJ

## ACKNOWLEDGMENTS

The authors thank Dr. Marianne Wessling-Resnick (Harvard School of Public Health, Boston, MA, USA) for providing insightful suggestions for the manuscript. This work was supported by the U.S. National Institutes of Health (NIH) National Institute of Environmental Health Sciences Grant K99/R00 ES024340 (to Y.A.S.), University of Michigan Protein Folding Disease Initiative grant (to Y.A.S.), and NIH National Institute of Neurological Disorders and Stroke Grant R01 NS089896 (to S.I.). The authors declare no conflicts of interest.

## AUTHOR CONTRIBUTIONS

Y.-A. Seo designed the research; E.-K. Choi and Y.A. Seo performed the experiments; E.-K. Choi, T.-T. Nguyen, S. Iwase, and Y.A. Seo analyzed data; S. Iwase and Y.A. Seo wrote the manuscript; and S. Iwase and Y.A. Seo contributed new reagents or analytic tools.

## REFERENCES

1. Feder, J. N., Gnirke, A., Thomas, W., Tsuchihashi, Z., Ruddy, D. A., Basava, A., Dormishian, F., Domingo, R., Jr., Ellis, M. C., Fullan, A., Hinton, L. M., Jones, N. L., Kimmel, B. E., Kronmal, G. S., Lauer, P., Lee, V. K., Loeb, D. B., Mapa, F. A., McClelland, E., Meyer, N. C., Mintier, G. A., Moeller, N., Moore, T., Morikang, E., Prass, C. E., Quintana, L., Starnes, S. M., Schatzman, R. C., Brunke, K. J., Drayna, D. T., Risch, N. J., Bacon, B. R., and Wolff, R. K. (1996) A novel MHC class I-like gene is mutated in patients with hereditary haemochromatosis. *Nat. Genet.* **13**, 399–408
2. Powell, L. W., Seckington, R. C., and Deugnier, Y. (2016) Haemochromatosis. *Lancet* **388**, 706–716
3. Kawabata, H., Yang, R., Hirama, T., Vuong, P. T., Kawano, S., Gombart, A. F., and Koeffler, H. P. (1999) Molecular cloning of transferrin receptor 2. A new member of the transferrin receptor-like family. *J. Biol. Chem.* **274**, 20826–20832
4. Pietrangelo, A., Caleffi, A., and Corradini, E. (2011) Non-HFE hepatic iron overload. *Semin. Liver Dis.* **31**, 302–318
5. Abboud, S., and Haile, D. J. (2000) A novel mammalian iron-regulated protein involved in intracellular iron metabolism. *J. Biol. Chem.* **275**, 19906–19912
6. Donovan, A., Lima, C. A., Pinkus, J. L., Pinkus, G. S., Zon, L. I., Robine, S., and Andrews, N. C. (2005) The iron exporter ferroportin/Slc40a1 is essential for iron homeostasis. *Cell Metab.* **1**, 191–200
7. McKie, A. T., Marciani, P., Rolfs, A., Brennan, K., Wehr, K., Barrow, D., Miret, S., Bomford, A., Peters, T. J., Farzaneh, F., Hediger, M. A., Hentze, M. W., and Simpson, R. J. (2000) A novel duodenal iron-regulated transporter, IREG1, implicated in the basolateral transfer of iron to the circulation. *Mol. Cell* **5**, 299–309
8. Nemeth, E., Tuttle, M. S., Powelson, J., Vaughn, M. B., Donovan, A., Ward, D. M., Ganz, T., and Kaplan, J. (2004) Hepcidin regulates cellular iron efflux by binding to ferroportin and inducing its internalization. *Science* **306**, 2090–2093
9. Qiao, B., Sugianto, P., Fung, E., Del-Castillo-Rueda, A., Moran-Jimenez, M. J., Ganz, T., and Nemeth, E. (2012) Hepcidin-induced endocytosis of ferroportin is dependent on ferroportin ubiquitination. *Cell Metab.* **15**, 918–924
10. Pietrangelo, A. (2017) Ferroportin disease: pathogenesis, diagnosis and treatment. *Haematologica* **102**, 1972–1984
11. McKie, A. T., and Barlow, D. J. (2004) The SLC40 basolateral iron transporter family (IREG1/ferroportin/MTP1). *Pflugers Arch.* **447**, 801–806
12. Madejczyk, M. S., and Ballatori, N. (2012) The iron transporter ferroportin can also function as a manganese exporter. *Biochim. Biophys. Acta* **1818**, 651–657
13. Mitchell, C. J., Shawki, A., Ganz, T., Nemeth, E., and Mackenzie, B. (2014) Functional properties of human ferroportin, a cellular iron exporter reactive also with cobalt and zinc. *Am. J. Physiol. Cell Physiol.* **306**, C450–C459
14. Yin, Z., Jiang, H., Lee, E. S., Ni, M., Erikson, K. M., Milatovic, D., Bowman, A. B., and Aschner, M. (2010) Ferroportin is a manganese-responsive protein that decreases manganese cytotoxicity and accumulation. *J. Neurochem.* **112**, 1190–1198
15. Li, X., Xie, J., Lu, L., Zhang, L., Zou, Y., Wang, Q., Luo, X., and Li, S. (2013) Kinetics of manganese transport and gene expressions of manganese transport carriers in Caco-2 cell monolayers. *Biometals* **26**, 941–953
16. Horning, K. J., Caito, S. W., Tipps, K. G., Bowman, A. B., and Aschner, M. (2015) Manganese is essential for neuronal Health. *Annu. Rev. Nutr.* **35**, 71–108
17. Milatovic, D., Zaja-Milatovic, S., Gupta, R. C., Yu, Y., and Aschner, M. (2009) Oxidative damage and neurodegeneration in manganese-induced neurotoxicity. *Toxicol. Appl. Pharmacol.* **240**, 219–225
18. Stanwood, G. D., Leitch, D. B., Savchenko, V., Wu, J., Fitsanakis, V. A., Anderson, D. J., Stankowski, J. N., Aschner, M., and McLaughlin, B. (2009) Manganese exposure is cytotoxic and alters dopaminergic and GABAergic neurons within the basal ganglia. *J. Neurochem.* **110**, 378–389
19. Seo, Y. A., and Kelleher, S. L. (2010) Functional analysis of two single nucleotide polymorphisms in SLC30A2 (ZnT2): implications for mammary gland function and breast disease in women. *Physiol. Genomics* **42A**, 219–227
20. Seo, Y. A., Lopez, V., and Kelleher, S. L. (2011) A histidine-rich motif mediates mitochondrial localization of ZnT2 to modulate mitochondrial function. *Am. J. Physiol. Cell Physiol.* **300**, C1479–C1489
21. Choi, E. K., Nguyen, T. T., Gupta, N., Iwase, S., and Seo, Y. A. (2018) Functional analysis of SLC39A8 mutations and their implications for manganese deficiency and mitochondrial disorders. *Sci. Rep.* **8**, 3163
22. Dunn, K. W., Kamocka, M. M., and McDonald, J. H. (2011) A practical guide to evaluating colocalization in biological microscopy. *Am. J. Physiol. Cell Physiol.* **300**, C723–C742
23. Seo, Y. A., Li, Y., and Wessling-Resnick, M. (2013) Iron depletion increases manganese uptake and potentiates apoptosis through ER stress. *Neurotoxicology* **38**, 67–73
24. Seo, Y. A., Kumara, R., Wetli, H., and Wessling-Resnick, M. (2016) Regulation of divalent metal transporter-1 by serine phosphorylation. *Biochem. J.* **473**, 4243–4254
25. McCarthy, R. C., and Kosman, D. J. (2014) Glial cell ceruloplasmin and hepcidin differentially regulate iron efflux from brain microvascular endothelial cells. *PLoS One* **9**, e89003
26. Seo, Y. A., and Wessling-Resnick, M. (2015) Ferroportin deficiency impairs manganese metabolism in flatiron mice. *FASEB J.* **29**, 2726–2733
27. Aschemeyer, S., Qiao, B., Stefanova, D., Valore, E. V., Sek, A. C., Ruwe, T. A., Vieth, K. R., Jung, G., Casu, C., Rivella, S., Jormakka, M., Mackenzie, B., Ganz, T., and Nemeth, E. (2018) Structure-function analysis of ferroportin defines the binding site and an alternative mechanism of action of hepcidin. *Blood* **131**, 899–910
28. Schimanski, L. M., Drakesmith, H., Merryweather-Clarke, A. T., Viprakasit, V., Edwards, J. P., Sweetland, E., Bastin, J. M., Cowley, D., Chinthammitr, Y., Robson, K. J., and Townsend, A. R. (2005) In vitro functional analysis of human ferroportin (FPN) and hemochromatosis-associated FPN mutations. *Blood* **105**, 4096–4102
29. Callebaut, I., Joubrel, R., Pissard, S., Kannengiesser, C., Gérolami, V., Ged, C., Cadet, E., Cartault, F., Ka, C., Gourlaouen, I., Gourhant, L., Oudin, C., Goossens, M., Grandchamp, B., De Verneuil, H., Rochette, J., Férec, C., and Le Gac, G. (2014) Comprehensive functional annotation of 18 missense mutations found in suspected hemochromatosis type 4 patients. *Hum. Mol. Genet.* **23**, 4479–4490
30. Détivaud, L., Island, M. L., Jouanolle, A. M., Ropert, M., Bardou-Jacquet, E., Le Lan, C., Mosser, A., Leroyer, P., Deugnier, Y., David, V., Brissot, P., and Loréal, O. (2013) Ferroportin diseases: functional studies, a link between genetic and clinical phenotype. *Hum. Mutat.* **34**, 1529–1536
31. Le Gac, G., Ka, C., Joubrel, R., Gourlaouen, I., Lehn, P., Mornon, J. P., Férec, C., and Callebaut, I. (2013) Structure-function analysis of the human ferroportin iron exporter (SLC40A1): effect of hemochromatosis type 4 disease mutations and identification of critical residues. *Hum. Mutat.* **34**, 1371–1380
32. Fernandes, A., Preza, G. C., Phung, Y., De Domenico, I., Kaplan, J., Ganz, T., and Nemeth, E. (2009) The molecular basis of hepcidin-resistant hereditary hemochromatosis. *Blood* **114**, 437–443
33. Wallace, D. F., Harris, J. M., and Subramaniam, V. N. (2010) Functional analysis and theoretical modeling of ferroportin reveals clustering of mutations according to phenotype. *Am. J. Physiol. Cell Physiol.* **298**, C75–C84
34. Gonçalves, A. S., Muzeau, F., Blaybel, R., Hetet, G., Driss, F., Delaby, C., Canonne-Hergaux, F., and Beaumont, C. (2006) Wild-type and mutant ferroportins do not form oligomers in transfected cells. *Biochem. J.* **396**, 265–275

35. Mukhopadhyay, S., Bachert, C., Smith, D. R., and Linstedt, A. D. (2010) Manganese-induced trafficking and turnover of the cis-Golgi glycoprotein GPP130. *Mol. Biol. Cell* **21**, 1282–1292
36. Biedler, J. L., Helson, L., and Spengler, B. A. (1973) Morphology and growth, tumorigenicity, and cytogenetics of human neuroblastoma cells in continuous culture. *Cancer Res.* **33**, 2643–2652
37. Wu, Z., Zhu, Y., Cao, X., Sun, S., and Zhao, B. (2014) Mitochondrial toxic effects of Aβ through mitofusins in the early pathogenesis of Alzheimer's disease. *Mol. Neurobiol.* **50**, 986–996
38. Zhu, Y., Hoell, P., Ahlemeyer, B., Sure, U., Bertalanffy, H., and Krieglstein, J. (2007) Implication of PTEN in production of reactive oxygen species and neuronal death in in vitro models of stroke and Parkinson's disease. *Neurochem. Int.* **50**, 507–516
39. Leyva-Illades, D., Chen, P., Zogzas, C. E., Hutchens, S., Mercado, J. M., Swaim, C. D., Morrisett, R. A., Bowman, A. B., Aschner, M., and Mukhopadhyay, S. (2014) SLC30A10 is a cell surface-localized manganese efflux transporter, and parkinsonism-causing mutations block its intracellular trafficking and efflux activity. *J. Neurosci.* **34**, 14079–14095
40. Nishito, Y., Tsuji, N., Fujishiro, H., Takeda, T. A., Yamazaki, T., Teranishi, F., Okazaki, F., Matsunaga, A., Tuschl, K., Rao, R., Kono, S., Miyajima, H., Narita, H., Himeno, S., and Kambe, T. (2016) Direct comparison of manganese detoxification/efflux proteins and molecular characterization of ZnT10 protein as a manganese transporter. *J. Biol. Chem.* **291**, 14773–14787
41. Li, J., Ma, Z., Shi, M., Malty, R. H., Aoki, H., Minic, Z., Phanse, S., Jin, K., Wall, D. P., Zhang, Z., Urban, A. E., Hallmayer, J., Babu, M., and Snyder, M. (2015) Identification of human neuronal protein complexes reveals biochemical activities and convergent mechanisms of action in autism spectrum disorders. *Cell Syst.* **1**, 361–374
42. De Domenico, I., Ward, D. M., Nemeth, E., Vaughn, M. B., Musci, G., Ganz, T., and Kaplan, J. (2005) The molecular basis of ferroportin-linked hemochromatosis. *Proc. Natl. Acad. Sci. USA* **102**, 8955–8960
43. McDonald, C. J., Wallace, D. F., Ostini, L., Bell, S. J., Demediuk, B., and Subramaniam, V. N. (2011) G80S-linked ferroportin disease: classical ferroportin disease in an Asian family and reclassification of the mutant as iron transport defective. *J. Hepatol.* **54**, 538–544
44. Rice, A. E., Mendez, M. J., Hokanson, C. A., Rees, D. C., and Björkman, P. J. (2009) Investigation of the biophysical and cell biological properties of ferroportin, a multipass integral membrane protein iron exporter. *J. Mol. Biol.* **386**, 717–732
45. Seo, Y. A., Elkhader, J. A., and Wessling-Resnick, M. (2016) Distribution of manganese and other biometals in flatiron mice. *Biometals* **29**, 147–155
46. Chen, P., Chakraborty, S., Mukhopadhyay, S., Lee, E., Paoliello, M. M., Bowman, A. B., and Aschner, M. (2015) Manganese homeostasis in the nervous system. *J. Neurochem.* **134**, 601–610
47. Guilarte, T. R. (2010) Manganese and Parkinson's disease: a critical review and new findings. *Environ. Health Perspect.* **118**, 1071–1080
48. Racette, B. A., McGee-Minnich, L., Moerlein, S. M., Mink, J. W., Videen, T. O., and Perlmutter, J. S. (2001) Welding-related parkinsonism: clinical features, treatment, and pathophysiology. *Neurology* **56**, 8–13
49. Wu, L. J., Leenders, A. G., Cooperman, S., Meyron-Holtz, E., Smith, S., Land, W., Tsai, R. Y., Berger, U. V., Sheng, Z. H., and Rouault, T. A. (2004) Expression of the iron transporter ferroportin in synaptic vesicles and the blood-brain barrier. *Brain Res.* **1001**, 108–117
50. McCarthy, R. C., and Kosman, D. J. (2015) Iron transport across the blood-brain barrier: development, neurovascular regulation and cerebral amyloid angiopathy. *Cell. Mol. Life Sci.* **72**, 709–727
51. Quadri, M., Federico, A., Zhao, T., Breedveld, G. J., Battisti, C., Delnooz, C., Severijnen, L. A., Di Toro Mammarella, L., Mignarri, A., Monti, L., Sanna, A., Lu, P., Punzo, F., Cossu, G., Willemsen, R., Rasi, F., Oostra, B. A., van de Warrenburg, B. P., and Bonifati, V. (2012) Mutations in SLC30A10 cause parkinsonism and dystonia with hypermanganesemia, polycythemia, and chronic liver disease. *Am. J. Hum. Genet.* **90**, 467–477
52. Tuschl, K., Clayton, P. T., Gospe, S. M., Jr., Gulab, S., Ibrahim, S., Singhi, P., Aulakh, R., Ribeiro, R. T., Barsottini, O. G., Zaki, M. S., Del Rosario, M. L., Dyack, S., Price, V., Rideout, A., Gordon, K., Wevers, R. A., Chong, W. K., and Mills, P. B. (2012) Syndrome of hepatic cirrhosis, dystonia, polycythemia, and hypermanganesemia caused by mutations in SLC30A10, a manganese transporter in man. *Am. J. Hum. Genet.* **90**, 457–466
53. Bosomworth, H. J., Thornton, J. K., Coneyworth, L. J., Ford, D., and Valentine, R. A. (2012) Efflux function, tissue-specific expression and intracellular trafficking of the Zn transporter ZnT10 indicate roles in adult Zn homeostasis. *Metallomics* **4**, 771–779
54. DeWitt, M. R., Chen, P., and Aschner, M. (2013) Manganese efflux in Parkinsonism: insights from newly characterized SLC30A10 mutations. *Biochem. Biophys. Res. Commun.* **432**, 1–4
55. Liu, X. B., Yang, F., and Haile, D. J. (2005) Functional consequences of ferroportin 1 mutations. *Blood Cells Mol. Dis.* **35**, 33–46
56. Lok, C. Y., Merryweather-Clarke, A. T., Viprakasit, V., Chinthammitr, Y., Srichairatanakool, S., Limwongse, C., Oleesky, D., Robins, A. J., Hudson, J., Wai, P., Premawardhena, A., de Silva, H. J., Dassanayake, A., McKeown, C., Jackson, M., Gama, R., Khan, N., Newman, W., Banait, G., Chilton, A., Wilson-Morkeh, I., Weatherall, D. J., and Robson, K. J. (2009) Iron overload in the Asian community. *Blood* **114**, 20–25
57. Corradini, E., Montosi, G., Ferrara, F., Caleffi, A., Pignatti, E., Barelli, S., Garuti, C., and Pietrangelo, A. (2005) Lack of enterocyte iron accumulation in the ferroportin disease. *Blood Cells Mol. Dis.* **35**, 315–318
58. Pietrangelo, A., Corradini, E., Ferrara, F., Vegetti, A., De Jong, G., Luca Abbati, G., Paolo Arcuri, P., Martinelli, S., and Cerofolini, E. (2006) Magnetic resonance imaging to identify classic and nonclassic forms of ferroportin disease. *Blood Cells Mol. Dis.* **37**, 192–196
59. Cunat, S., Giansily-Blaizot, M., Bismuth, M., Blanc, F., Dereure, O., Larrey, D., Quellec, A. L., Pouderoux, P., Rose, C., Raingeard, I., Renard, E., Schved, J. F., and Aguilar-Martinez, P.; CHU Montpellier AOI 2004 Working Group. (2007) Global sequencing approach for characterizing the molecular background of hereditary iron disorders. *Clin. Chem.* **53**, 2060–2069
60. Hetet, G., Devaux, I., Soufir, N., Grandchamp, B., and Beaumont, C. (2003) Molecular analyses of patients with hyperferritinemia and normal serum iron values reveal both L ferritin IRE and 3 new ferroportin (slc11A3) mutations. *Blood* **102**, 1904–1910
61. Njajou, O. T., de Jong, G., Berghuis, B., Vaessen, N., Snijders, P. J., Goossens, J. P., Wilson, J. H., Breuning, M. H., Oostra, B. A., Heutink, P., Sandkuijl, L. A., and van Duijn, C. M. (2002) Dominant hemochromatosis due to N144H mutation of SLC11A3: clinical and biological characteristics. *Blood Cells Mol. Dis.* **29**, 439–443
62. Rosmorduc, O., Wendum, D., Arrivé, L., Elnaggar, A., Ennibi, K., Hannoun, L., Charlotte, F., Grangé, J. D., and Poupon, R. (2008) Phenotypic expression of ferroportin disease in a family with the N144H mutation. *Gastroenterol. Clin. Biol.* **32**, 321–327
63. Arden, K. E., Wallace, D. F., Dixon, J. L., Summerville, L., Searle, J. W., Anderson, G. J., Ramm, G. A., Powell, L. W., and Subramaniam, V. N. (2003) A novel mutation in ferroportin1 is associated with haemochromatosis in a Solomon Islands patient. *Gut* **52**, 1215–1217
64. Sham, R. L., Phatak, P. D., West, C., Lee, P., Andrews, C., and Beutler, E. (2005) Autosomal dominant hereditary hemochromatosis associated with a novel ferroportin mutation and unique clinical features. *Blood Cells Mol. Dis.* **34**, 157–161
65. Sham, R. L., Phatak, P. D., Nemeth, E., and Ganz, T. (2009) Hereditary hemochromatosis due to resistance to hepcidin: high hepcidin concentrations in a family with C326S ferroportin mutation. *Blood* **114**, 493–494

*Received for publication April 30, 2018.*
*Accepted for publication August 27, 2018.*